Computer Science and Information Systems 23(2):861–884 https://doi.org/10.2298/CSIS251029015C

HAQCCN: A Hybrid Quantum–Classical Convolutional Network with Asymmetric Kernels for Remote Sensing Image Classification

Lianghai Chen[1,2], Yuzhen Liu[1,3], Yi Lu[1,4], Xiaoliang Wang[1,5] and Huaning Song[6]

[1] School of Computer Science and Engineering, Hunan University of Science and Technology
Xiangtan, China
Sanya Institute of Hunan University of Science and Technology
Sanya, China
[2] chenlh@mail.hnust.edu.cn
[3] yzhenliu@126.com
[4] 24010502004@mail.hnust.edu.cn
[5] fengwxl@hnust.edu.cn (corresponding author)
[6] School of Artificial Intelligence and Manufacturing,Hechi University
Hechi,Guangxi
shn_2008@163.com (corresponding author)

Abstract. Remote sensing image classification is a fundamental task for Earth observation and environmental monitoring. However, conventional convolutional neural networks (CNNs) are limited by computational capacity and struggle to efficiently process the rapidly growing volume of remote sensing data. To address this limitation, we propose HAQCCN (Hybrid Asymmetric Quantum–Classical Convolutional Network), a novel hybrid architecture that integrates quantum computation into the classical convolutional framework through asymmetric quantum convolutional circuits. In HAQCCN, the asymmetric quantum circuits enable a limited number of qubits to process more classical data while maintaining excellent feature extraction capability. Experiments conducted on the IBM Qiskit platform using the Overhead-MNIST, PatternNet, and RSI-CB256 datasets demonstrate that HAQCCN outperforms conventional CNNs and existing quantum models. Furthermore, we systematically investigate the effects of encoding schemes, the number of quantum convolutional kernels, and the number of qubits on model performance, confirming the effectiveness and scalability of the proposed method for remote sensing image classification.

Keywords: Remote Sensing Image Classification, Quantum Computing, Convolutional Neural Networks, Quantum Convolutional Network, Feature Extraction, Deep Learning.

1. Introduction

Remote sensing image classification, as a core task in the field of Earth Observation (EO) [1], holds significant importance in multiple practical applications, including environmental monitoring [2], urban planning [3], hydrological observation [4], and disaster response [5]. Along with the remarkable progress achieved in satellite and sensor technologies, the volume of multispectral and high-resolution remote sensing data

has been growing exponentially across spatial, temporal, and spectral dimensions, marking EO's full transition into the era of big data [6]. While the availability of such rich data provides a solid foundation for fine-grained analysis, it also leads to increasingly severe challenges in computational cost, storage demand, and energy consumption [7]. Convolutional neural networks (CNNs), as the most prominent deep learning technique, have demonstrated high effectiveness in remote sensing image classification [8–10]. However, their training and inference phases typically require a large number of parameters and considerable computational resources. This poses significant limitations for deployment on resource-constrained embedded systems, satellite onboard processing, or applications requiring low-latency responses, thereby restricting their practical feasibility in real-world engineering scenarios [7, 10, 11]. To address these challenges, it is imperative to explore alternative computational paradigms. Quantum computing, with its inherent potential for high-efficiency information processing, offers a promising direction to overcome the aforementioned limitations [12–14].

Quantum computing, owing to its intrinsic properties such as parallelism and quantum entanglement, has been regarded as a promising paradigm for alleviating the computational bottlenecks of classical computing [12]. It has demonstrated potential across various domains, including data processing [15, 16], data classification [17], image segmentation [18, 19], model optimization [20], computer security [21, 22] and computational acceleration [23]. Under the current era of Noisy Intermediate-Scale Quantum (NISQ) devices, Quantum Machine Learning (QML) has emerged as an active research area [24], seeking to exploit Parameterized Quantum Circuits (PQCs) or quantum feature mappings to enhance data representation and computational efficiency.Within this context, quantum computing is increasingly viewed as a potential pathway to overcome the limitations of conventional image processing techniques [12]. In particular, QML models based on PQCs or quantum annealers have exhibited unique advantages in high-dimensional feature extraction and nonlinear transformation [25, 26]. Specifically, quantum convolution—by mapping local convolutional operations onto quantum circuits—has shown promise in reducing the number of trainable parameters while enabling efficient parallel processing [27]. In this regard, several representative studies have proposed structural optimization schemes for quantum models from different perspectives. For instance, Meng et al. [28] and Wu et al. [29] respectively investigated quantum approaches for graph data processing and image analysis. The Quantum Spatial Graph Convolutional Network (QSGCN) proposed in [28] integrates PQCs into graph neural networks and provides an in-depth analysis of trainability issues, with particular attention to the barren plateau problem, thereby offering a new approach for handling non-Euclidean structured data. Meanwhile,Yang et al. [30] focused on the development of Quantum Convolutional Neural Networks (QCNNs), employing the Multi-scale Entanglement Renormalization Ansatz (MERA) to effectively reduce computational complexity. They further incorporated quantum convolutional modules into classical convolutional architectures to construct hybrid models, demonstrating their effectiveness on the MNIST dataset.

Collectively, these studies aim to improve the trainability and efficiency of quantum neural networks from different data structure perspectives. However, existing quantum image representation and encoding methods often incur significant overhead in terms of qubit count and gate operations, making them difficult to apply directly to remote sensing imagery. Moreover, most existing hybrid quantum–classical vision models are validated

only on simple, small-scale datasets and typically rely on extensive classical preprocessing [31], thereby limiting their generalization capability and end-to-end trainability in real-world remote sensing applications.

Given the aforementioned context, a key challenge lies in achieving an effective trade-off between limited quantum computational resources and the demands of large-scale remote sensing image processing, while ensuring model effectiveness. Developing a hybrid model that can operate under Noisy Intermediate-Scale Quantum (NISQ) conditions and possess practical engineering applicability remains an urgent and unresolved problem.

To address these challenges, this study proposes a Hybrid Asymmetric Quantum-Classical Convolutional Network (HAQCCN) tailored for remote sensing image classification. At the encoding stage, we introduce an asymmetric encoding scheme in which the input image is divided into multiple local patches. Each patch is projected and embedded into a limited number of qubits via controlled rotation gates. Through a specially designed encoding module, the proposed method enables the representation of data exceeding the available qubit count while maintaining model performance. This design substantially reduces qubit requirements and preserves spatial and texture information at the local scale.

During feature extraction, the parallel quantum convolutional units employ parameterized entangling layers to perform quantum-level transformations on local features. In the subsequent stages, classical aggregation and classification modules are utilized to fuse and discriminate the extracted quantum features, forming a differentiable end-to-end hybrid training pipeline that allows joint optimization between quantum and classical components.

To evaluate the effectiveness and generalization capability of the proposed AQCN, comprehensive experiments were conducted on three publicly available remote sensing datasets Overhead-MNIST [32], PatternNet [33], and RSI-CB256 [34]. These datasets encompass varying spatial resolutions and spectral characteristics, thereby reflecting the diversity of representative remote sensing scenarios. Experimental results demonstrate that, even in the presence of quantum noise, our model outperforms both classical CNN baselines and existing quantum-based approaches in classification accuracy. Furthermore, ablation studies covering encoding strategies, qubit numbers, and convolutional kernel sensitivity analyses confirm that HAQCCN exhibits strong robustness and provides a flexible performance–cost trade-off.

The main contributions of this work are summarized as follows:

1. Asymmetric Quantum Encoding Model: We propose an asymmetric quantum encoding scheme that effectively enhances the capacity of qubits to process classical information, providing a novel perspective for quantum encoding.

2. Quantum Convolutional Layer: A new quantum convolutional layer is proposed, utilizing a kernel composed of U3 rotation gates and cross-qubit CNOT gates. This structure enhances feature interaction and entanglement representation, enabling richer feature extraction with limited qubits and achieving superior performance in remote sensing image classification.

3. Systematic Analysis of Quantum Design Factors: This study investigates the impacts of quantum encoding strategies, quantum convolutional kernels, and qubit numbers on model classification performance, offering valuable insights for future research on quantum models.

The organization of this paper is as follows: Chapter 2 presents a detailed description of the proposed model's overall framework and implementation, including data preprocessing and encoding strategies, design and operational procedures of quantum convolutional kernels, measurement protocols, and the subsequent classical dense layer architecture, thereby constructing a classification model based on AQCN. Chapter 3 introduces the datasets and data processing procedures, describes the comparative models, outlines the experimental platform and configurations, and presents the experimental results. Chapter 4 provides a detailed analysis of the results from Chapter 3, discusses implications for current research, identifies limitations, and suggests potential improvements. Chapter 5 provides a summary of the paper and discusses potential directions for future research.

Through this work, we aim to provide both methodological and engineering references for the practical application of quantum computing in remote sensing image analysis, thereby promoting the development of efficient and deployable solutions for Earth Observation tasks in the context of big data.

2. Materials and Methods

This study proposes a hybrid QC-CNN model, designed to perform remote sensing image classification using supervised deep learning methods by specifically leveraging rotational encoding techniques. As illustrated in Fig. 1, the proposed QC-CNN model consists of two sequential components. The quantum circuit component efficiently extracts salient features from the input images, while the classical component subsequently performs the final classification task.

Specifically, the model comprises four main modules: (1) data processing, (2) quantum convolution, (3) measurement layer, and (4) dense layer.

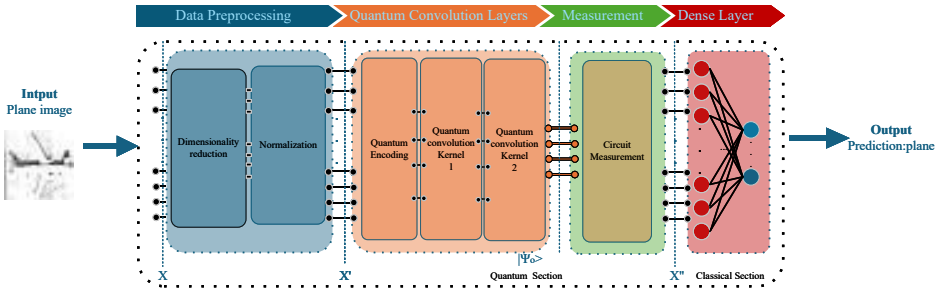

Fig. 1. Overall architecture of the HAQCCN model: 1) Input image data, perform dimensionality reduction and normalization 2) Use the quantum coding circuit to convert the image data into a quantum state, and then pass it through two quantum convolution kernels 3) The circuit measurement layer is responsible for converting the data processed by the quantum convolution kernel into classical data 4) The measured data is sent to the dense layer for classification, and the classification results of the model are output

2.1. Data Preprocessing

During the data preprocessing stage, the original image data is first subjected to dimensionality reduction to reduce computational complexity. Subsequently, the feature values are normalized to the interval $[0, \pi]$ and transformed into rotation angles $\theta_0, \theta_1, \theta_2, \theta_3, \theta_4, \ldots,$ enabling their direct use as rotation parameters for quantum RX gates. This procedure effectively performs the encoding transformation from classical data to quantum states.

2.2. Quantum Convolution Layers

Data Encoding: In this section, we will introduce the quantum coding circuit we use, the specific structure of which is shown in Fig. 2. In quantum computing, rotation gates [35] are a class of single-qubit gates that rotate quantum states around a specific axis on the Bloch sphere. we employ the RX rotation gate for encoding, which can be described as:

$$\mathrm{R_X}(\theta) = \mathrm{e}^{-\mathrm{i}\frac{\theta}{2}\mathrm{X}} \tag{1}$$

Here, X denotes the Pauli-X matrix:

$$\begin{bmatrix} 0 & 1 \\ 1 & 0 \end{bmatrix} \tag{2}$$

When the RX rotation gate is applied to a qubit in the state $|0\rangle$ or $|1\rangle$, its action is as follows: Applied to $|0\rangle$:

$$R_X(\theta)|0\rangle = \cos\frac{\theta}{2}|0\rangle - i\sin\frac{\theta}{2}|1\rangle \tag{3}$$

Applied to $|1\rangle$:

$$R_X(\theta)|1\rangle = -i\sin\frac{\theta}{2}|0\rangle + \cos\frac{\theta}{2}|1\rangle \tag{4}$$

In the quantum encoding layer, CNOT gates are introduced to perform simple entanglement operations, enabling the input quantum states to the convolutional layer to represent entangled states of a convolutional block. The controlled-NOT(CNOT) gate [36], as a fundamental two-qubit operation, plays a crucial role in the transmission of information. CNOT gates can generate quantum entanglement, allowing information between different qubits to interact via quantum coherence, thereby facilitating more efficient feature mapping. Moreover, within the quantum convolutional layer, CNOT gates are employed to establish correlations between quantum channels, enabling features to propagate across qubits and enhancing the expressive capacity of the model. Compared with classical convolution, this quantum-based approach not only accelerates computation but also leverages quantum properties to improve the model's generalization capability.

The CNOT gate is a type of controlled gate that operates on two qubits: a control qubit and a target qubit. Its operational rule is as follows: if the control qubit is in the state $|0\rangle$, the target qubit remains unchanged; if the control qubit is in the state $|1\rangle$, the target qubit undergoes an X (NOT) operation, i.e., $|0\rangle \leftrightarrow |1\rangle$.

Mathematically, the action of the CNOT gate can be represented as:

$$|c, t\rangle \rightarrow |c, t \oplus c\rangle \tag{5}$$

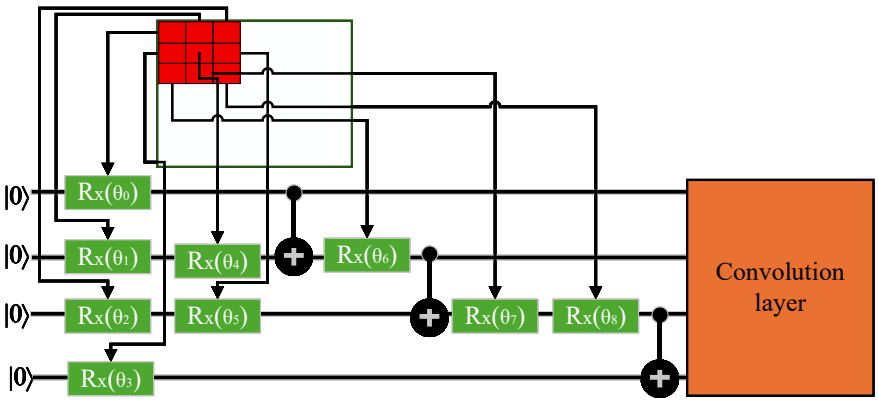

Fig. 2. Quantum coding circuit: The red block represents a 3*3 data block in classical data. Each pixel data enters the quantum circuit through the RX rotation gate (green part). The coding circuit also uses three CNOT gates (black) to entangle the data. The encoded data is finally sent to the quantum coding layer.

Here, c represents the value of the control qubit, t represents the value of the target qubit, and $\oplus$ denotes the bitwise XOR operation.

In our circuit, three CNOT gates are employed to generate entangled states among the data. These three CNOT gates connect four qubits, creating entanglement across all four qubits and enhancing the expressive capability of the quantum circuit for the input data. In our convolutional circuit, by strategically placing the RX encoding gates at key positions within the quantum circuit, four qubits are able to encode nine classical data points. In contrast, other studies on quantum convolution typically utilize a number of qubits equal to the number of convolutional data points.

Next, we provide a detailed analysis of our encoding circuit.

Let the initial state be:

$$|\psi_0\rangle = |0000\rangle \tag{6}$$

Subsequently, rotation gates are applied to the four qubits with rotation angles $\theta_0, \theta_1, \theta_2, \theta_3$. The RX gates modify the state of each qubit, resulting in the system entering the state:

$$|\psi_1\rangle = R(\theta_0)R(\theta_1)R(\theta_2)R(\theta_3)|\psi_0\rangle \tag{7}$$

The rotation operation $R_x(\theta)$ induces a corresponding rotation on each qubit, causing the qubits to enter a superposition state and thereby enabling subsequent quantum entanglement. On this basis, additional rotation gates $R_x(\theta_4)$ and $R_x(\theta_5)$ are applied to qubits q_1 and q_2, respectively, further adjusting the quantum states:

$$|\psi_2\rangle = IR(\theta_4)R(\theta_5)I|\psi_1\rangle \tag{8}$$

At this stage, the qubits are already in a more complex superposition state, laying the foundation for subsequent CNOT gate operations and quantum entanglement. In this step,

a CNOT gate is applied with q_0 as the control qubit and q_1 as the target qubit. If q_0 is in the state $|1\rangle$, the state of q_1 is flipped, thereby introducing quantum entanglement:

$$|\psi_3\rangle = \mathrm{CNOT}\,|\psi_2\rangle \tag{9}$$

Next, the rotation gate $R_x(\theta_6)$ is applied to q_1, altering its phase information and thereby affecting the coherence of the quantum state:

$$|\psi_4\rangle = \mathrm{IR}\,(\theta_6)\,II\,|\psi_3\rangle \tag{10}$$

At this stage, a CNOT gate is again applied with q_1 as the control qubit and q_2 as the target qubit. This step entangles qubits q_1 and q_2:

$$|\psi_5\rangle = \mathrm{CNOT}\,|\psi_4\rangle \tag{11}$$

The rotation gates $R_x(\theta_7)$ and $R_x(\theta_8)$ are applied to q_2 and q_3, respectively, to adjust the phases of the quantum states. Through these rotations, the coherence of the qubits can be precisely controlled:

$$\left|\psi^6\right\rangle = \mathrm{IIR}\,(\theta_7)\,I\,|\psi_5\rangle \tag{12}$$

$$|\psi_7\rangle = \mathrm{IIIR}\,(\theta_8)\,|\psi_6\rangle \tag{13}$$

Finally, a CNOT gate is applied with q_2 as the control qubit and q_3 as the target qubit. Through this operation, the quantum state of the entire system ultimately forms a complex multi-qubit entangled state:

$$|\psi_8\rangle = \mathrm{CNOT}\,|\psi_7\rangle \tag{14}$$

Through the aforementioned steps, we successfully employ a combination of rotation gates and CNOT gates to evolve the four-qubit quantum system from the initial state $|0000\rangle$ into a highly entangled quantum state $|\psi_8\rangle$, thereby completing the encoding process. The use of quantum-based encoding enables higher-dimensional representations compared with conventional machine learning methods [37, 38].

Quantum Convolution: The purpose of the quantum convolutional layer in the QC-CNN model is to perform convolution operations; this quantum layer is responsible for feature extraction and generating the corresponding feature maps.Our quantum convolution kernel is shown in Fig. 3.Within the convolutional layer, we introduce the U3 gate [39]. The U3 gate is a single-qubit gate and is considered the most general and powerful single-qubit operation. Its name derives from the fact that it is a unitary matrix parameterized by three angles. Conceptually, it can be regarded as a "universal" operation that performs arbitrary rotations on the Bloch sphere [40]. Almost any operation on a single qubit can be implemented using a single U3 gate. It has powerful expressive power, and its three learnable parameters make the quantum layer rich in adaptability.The U3 gate is represented by a 2×2 unitary matrix, and its standard matrix form is as follows:

$$U3(\theta, \phi, \lambda) = \begin{bmatrix} \cos(\theta/2) & -e^{i\lambda}\sin(\theta/2) \\ e^{i\phi}\sin(\theta/2) & e^{i(\phi+\lambda)}\cos(\theta/2) \end{bmatrix} \tag{15}$$

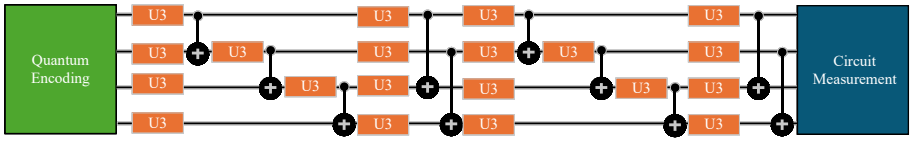

Fig. 3. Quantum convolution circuit: Processes data encoded by the quantum coding layer through two consecutive quantum convolution kernels. The orange one represents the U3 gate and the black one represents the CNOT gate. The processed data is captured and decoded by the measurement layer.

The U3 gate has three real parameters: θ (theta): Controls the rotation angle around the Y-axis. It determines the probability amplitude of the quantum state transitioning between the $|0\rangle$ and $|1\rangle$ basis states. ϕ (phi): The phase angle associated with the $|1\rangle$ state. λ (lambda): The phase angle associated with the $|0\rangle$ state. When the U3 gate is applied to a qubit:

$$\mathrm{U3}(\theta,\phi,\lambda)|0\rangle = \cos\frac{\theta}{2}|0\rangle + e^{i\phi}\sin\frac{\theta}{2}|1\rangle \tag{16}$$

$$\mathrm{U3}(\theta,\phi,\lambda)|1\rangle = -e^{i\lambda}\sin\frac{\theta}{2}|0\rangle + e^{i(\phi+\lambda)}\cos\frac{\theta}{2}|1\rangle \tag{17}$$

Our convolutional kernel, as illustrated in the Fig. 3, receives the output $|\psi_8\rangle$ from the encoding layer. We define:

$$|\psi_{\text{in}}\rangle = |\psi_8\rangle = \sum_{a,b,c,d\in\{0,1\}} \alpha_{a,b,c,d}|abcd\rangle \tag{18}$$

At the initial stage of the convolutional layer, four U3 gates are applied to the quantum states. These four U3 gates primarily perform a basic transformation on the encoded data:

$$|\psi_{\text{c1}}\rangle = \left[\mathrm{U3}_1\left(\theta_1,\phi_1,\lambda_1\right)\otimes\mathrm{U3}_2\left(\theta_2,\phi_2,\lambda_2\right)\otimes\mathrm{U3}_3\left(\theta_3,\phi_3,\lambda_3\right)\otimes\mathrm{U3}_4\left(\theta_4,\phi_4,\lambda_4\right)\right]|\psi_{\text{in}}\rangle \tag{19}$$

Subsequently, a CNOT gate is created between qubits q_0 and q_1 to enhance entanglement between them, and a U3 gate is applied to q_1 to further adjust its quantum state:

$$|\psi_{\text{c2}}\rangle = \left[\mathrm{I}\otimes\mathrm{U3}_2\left(\theta_6,\phi_6,\lambda_6\right)\otimes\mathrm{I}\otimes\mathrm{I}\right]\mathrm{CNOT}_{0,1}\,|\psi_{\text{c1}}\rangle \tag{20}$$

$$|\psi_{\text{c3}}\rangle = \mathrm{CNOT}_{2,3}\left[\left(\mathrm{I}\otimes\mathrm{I}\otimes\mathrm{U3}_2(\theta_6,\phi_6,\lambda_6)\otimes\mathrm{I}\right)\mathrm{CNOT}_{1,2}\,|\psi_{\text{c2}}\rangle\right] \tag{21}$$

The above operations complete the propagation of quantum features. Finally, a set of U3 gates is applied to make fine adjustments to the entire quantum state after feature extraction, and two CNOT gates are used to strengthen the correlations between the qubit pairs (q_0, q_2) and (q_1, q_3):

$$|\psi_{c4}\rangle = [\mathrm{U3}_0(\theta_7, \phi_7, \lambda_7) \otimes \mathrm{U3}_1(\theta_8, \phi_8, \lambda_8) \otimes \mathrm{U3}_2(\theta_9, \phi_9, \lambda_9) \otimes \mathrm{U3}_3(\theta_{10}, \phi_{10}, \lambda_{10})] |\psi_{c3}\rangle \tag{22}$$

$$|\psi_{\mathrm{out}}\rangle = \mathrm{CNOT}_{1,3}\mathrm{CNOT}_{0,2} |\psi_{c4}\rangle \tag{23}$$

At this stage, a quantum convolutional kernel is formed. In this study, the proposed model employs two of the aforementioned convolutional kernels to enhance the feature extraction capability of the model.

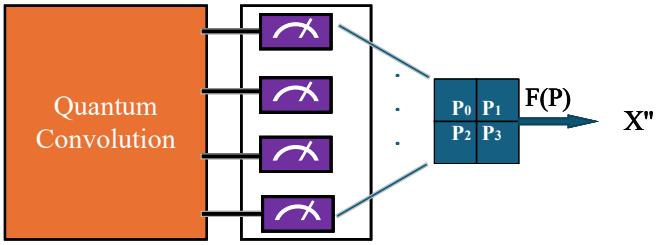

Fig. 4. In the measurement layer, we repeatedly run and measure the states of the four qubits, converting the measured value from F(P) to the value after this convolution

Measurement Layer: The quantum measurement layer, a core module of the Quantum Convolutional Neural Network (QCNN) whose structure is shown in Fig. 4, serves as a bridge between the quantum state space and the classical information space. It efficiently reduces the dimensionality of quantum data while preserving critical features. This layer transforms the quantum features extracted by the quantum convolutional layer into classically readable probability distributions through projective measurements, generalized measurements, or weak measurements, thereby supporting downstream tasks such as classification and regression. During this process, quantum measurement not only determines the efficiency of information extraction but also directly influences the expressive power and computational efficiency of the model through the combined effects of quantum state collapse and entanglement.

A measurable observable A, which is a Hermitian operator [41], can be expressed as:

$$A = \sum_i a_i P_i \tag{24}$$

Let the quantum state of the system be:

$$|\psi\rangle = \sum_i c_i |\varphi_i\rangle \tag{25}$$

The probability of obtaining the eigenvalue a_i upon measurement is given by:

$$P(a_i) = \langle\psi|P_i|\psi\rangle = |\langle\varphi_i|\psi\rangle|^2 \tag{26}$$

If the measurement outcome is a_i, the system collapses to the corresponding eigenstate:

$$|\psi'\rangle = \frac{\mathrm{P_i}|\psi\rangle}{\sqrt{\mathrm{P}\left(\mathrm{a_i}\right)}} = |\varphi_{\mathrm{i}}\rangle \tag{27}$$

After performing measurements on the four qubits, the expectation values of the four two-qubit pairs are obtained, as shown in Fig. 4. These four expectation values are computed as:

$$F(P) = \sum_{i=0}^{3} w_i P_i + b_i \tag{28}$$

and then fed into the subsequent classification layer, where w_i denotes the weights and b_i denotes the biases.

2.3. Dense Layer

After measuring the quantum layer, the results are fed into the dense layer of a classical deep learning model [42]. In a dense layer, each input node is connected to every output node, performing feature mapping through a linear transformation (i.e., a weighted sum plus a bias) followed by a nonlinear activation function. Dense layers are commonly employed to extract global features and accomplish classification tasks, particularly in the later stages of the network, where they map high-dimensional features to the target output dimensions, such as the probability distribution of class labels.

3. Experiment and Results

To evaluate the performance of our model in remote sensing image classification, we conducted comparative experiments with different models and designed additional experiments focused on our model to investigate the effects of various factors on its performance.

3.1. Data Preparation

In this study, we conducted experiments on five different Earth Observation (EO) datasets, namely Overhead-MNIST [32], PatternNet [33], and RSI-CB256 [34]. Due to the computational limitations of contemporary quantum simulators, we restricted our experiments to a subset of categories in each benchmark dataset. Additionally, we employed the Lanczos algorithm [43] to resize all labeled images in the datasets to 8×8 pixels.In the research of quantum convolutional networks, similar methods are widely employed for processing datasets [44–47].

The Overhead-MNIST [32] dataset consists of grayscale aerial images of 10 land-cover classes (e.g., ”car”, ”ship”, ”airplane”, etc.), each with a resolution of 28×28

pixels. The dataset contains 8,519 training samples and 1,065 testing samples. In our experiments, we selected six representative classes—"car", "ship", "airplane", "port", "helicopter", and "oilfield"—including all labeled images, totaling 5,098 samples for training. Additionally, 637 samples from the same classes were selected as an independent test set for performance evaluation. During the training phase, approximately 15% of the training samples were randomly allocated as a validation set, while the remaining samples were used for model training.

The PatternNet [33] dataset contains high-resolution remote sensing images from 38 categories, with approximately 800 samples per category, each of size 256×256 pixels. In our experiments, three representative classes—"coastal mansion", "parking lot", and "swimming pool"—were selected, and all corresponding samples were used. To evaluate the model, the samples were randomly divided into three non-overlapping sets: 70% for training, 15% for validation, and 15% for testing.

RSI-CB256 [34] is a global-scale remote sensing image dataset comprising 35 categories with over 24,000 images. In this study, five representative classes—"dry farm", "mangrove", "residential area", "snow mountain", and "storage room"—were selected for experiments, using all available samples in each class. All images have a resolution of 256×256 pixels. For experimental purposes, the dataset was randomly segmented into three exclusive subsets: 70% for training, 15% for validation, and 15% for testing.

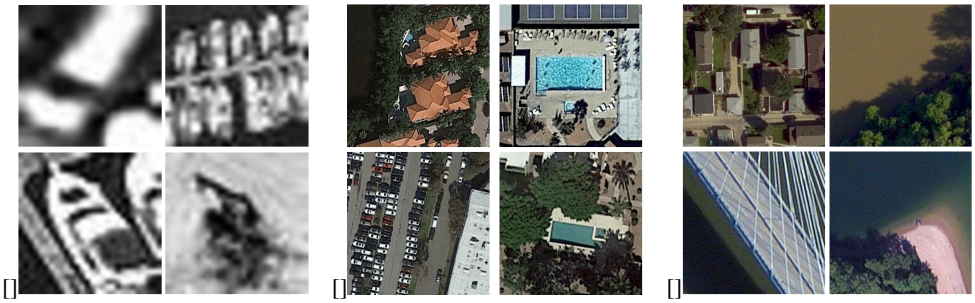

Fig. 5. The three datasets used in our experiments are: a) ovhead-mnist example b) patternNet example c) RSI-CB256 example

3.2. Model preparation

In our experiments, our model employs two quantum convolutional kernels for feature extraction. Additionally, we selected two classical convolutional schemes and four quantum convolutional schemes for comparison. The two classical models are CNN3 and DenseNet [48], where CNN3 corresponds to the classical counterpart of our model, utilizing average convolution. DenseNet includes an initial convolutional layer, two consecutive Dense blocks, a Transition Layer, and a final fully connected layer for classification.

In hybrid quantum–classical convolutional frameworks, classical data are encoded via single-qubit rotation gates and entangled through fixed circuits or CNOT gates [49]. While such methods exploit quantum superposition and entanglement for high-dimensional feature representation, limited qubits or deep circuits increase resource demands, training

complexity, and noise accumulation. The proposed method optimizes quantum kernel design and data encoding, enabling effective feature extraction with few qubits and shallow circuits. Compared to conventional approaches, it achieves higher convolutional efficiency and classification accuracy with low quantum overhead, while offering greater scalability across diverse inputs and convolutional structures.

From the perspectives of encoding, entanglement, and qubit count, we selected four existing Hybrid Quantum-Classical convolutional models for comparison.The four comparative quantum models are QCNN1 [45], QCNN2 [31], QCNN3 [30] and QCNN4 [50]. The model proposed by Fanfan [45] uses ten qubits encoded through H and RY gates and employs U3 gates to convolve the four input channels. It was evaluated on the Overhead-MNIST dataset [32]. The following three models all use four quantum bits to convolve four classical data.The model in [31] applies Hadamard (H) gates to establish entanglement and then uses RY gates to encode classical data into quantum states. The quantum convolutional model in [30] employs four qubits and integrates three types of encoding schemes. The model presented in [50] constructs the quantum circuit primarily by combining RY and CNOT gates to configure the circuit and generate entanglement. For a fair comparison across models and datasets in this work, we restrict all experiments to single-channel images.These selected models provide a comprehensive benchmark covering different qubit configurations, encoding strategies, and entanglement mechanisms, allowing a systematic evaluation of hybrid quantum-classical convolutional architectures and highlighting the potential advantages and limitations of each design in practical image processing tasks.

3.3. Experimental setup

Hardware and Software Environment: In our study, IBM's Qiskit platform [51] was used for model implementation and training. Qiskit, a major framework in quantum deep learning, enables the use of multiple simulator variants.Interested readers can refer to [52] for an in-depth discussion of different frameworks. Additionally, we used an Intel(R) Xeon(R) Gold 6458Q CPU and Nvidia A800 GPU to build a Qiskit simulation platform based on Ubuntu 22.04.5 LTS.

Experimental Setup: To ensure fairness in comparative experiments, all datasets were reduced to 8×8 using the Lanczos algorithm [43], and single-channel images were used for training. The number of epochs was set to 200, employing the cross-entropy loss function and the Adam optimizer [53]. Each training session was repeated three times, and the model that achieved the highest validation accuracy during training was employed for testing. The average test accuracy and its corresponding standard deviation were calculated for comparison and discussion. It is worth noting that, unlike [45, 54, 55], which use noiseless quantum simulators, our experiments introduce quantum noise during training to better simulate real quantum environments. Consequently, all quantum model experiments additionally incorporate the noise effects associated with running quantum models, compared with classical models.

Since the experiments are conducted on a quantum noise simulation platform, to better characterize the noise carried by the platform, we use four simple quantum circuits for the experiments. The circuits are shown in Figure 6 and mainly consist of H gates, RX gates, and CNOT gates. The H gates are used to test the noise in quantum superposition, the RX gates test the noise introduced by single-qubit rotation operations (such as RX, RY,

RZ, and U3 gates), and the CNOT gates test the noise in entangling operations. These circuits enable testing of both quantum entanglement and superposition, recording the noisy measurement outcomes on the experimental platform. Each experiment is repeated three times, and the mean and standard deviation of the results are calculated.

The experimental results are shown in Table 1, illustrating the impact of the experimental noise on quantum operations in our setup.Four simple quantum circuits based on the H gate, RX gate, and CNOT gate were designed for the experimental evaluation. The results indicate that, for circuits involving only single-qubit superposition operations, the measured outcomes agree well with the theoretical values, and the impact of noise remains minimal. In contrast, when CNOT-induced entanglement and RX-based rotations are introduced, the cumulative noise effects become significantly more pronounced, leading to larger deviations between measured and ideal results, as well as an expansion in the fluctuation range of the measurement data. This phenomenon highlights the platform's sensitivity to noise during two-qubit entanglement and dynamic rotational operations. Furthermore, a quantitative analysis of the platform's quantum noise was conducted to assess its impact on the execution of quantum circuits.

Based on the above settings, we conducted two main categories of experiments: comparative experiments and ablation studies. Specifically, five types of experiments were designed to evaluate model performance:

1) Comparative experiments across different models: This experiment aims to compare the performance of our model with six other models.

2) Performance comparison under different quantum encoding schemes: This experiment investigates how different encoding strategies affect the performance of our model.

3) Performance comparison under varying numbers of convolutional kernels: Since our model employs two quantum convolutional kernels, this experiment examines the influence of each kernel on model performance. 4) Performance comparison with different numbers of qubits: One of the primary goals of our proposed model is to reduce quantum resource consumption. Accordingly, we modified our model to a three-qubit quantum convolutional version to evaluate the effect of qubit quantity on model performance. 5) Assessment of the proposed quantum circuit's contribution to classification: In this experiment, the quantum component of our model is removed, and the preprocessed data is directly fed into the dense layer, effectively degrading the model to a fully connected neural network.

Among these five experiments, the first experiment utilizes the full dataset, whereas the subsequent experiments are conducted using the Overhead-MNIST and PatternNet datasets.

3.4. Experimental results

Model comparison performance analysis: We present the classification performance of different models in Table 2. As shown in Table 2, it is important to note that in Experiment 1, the configuration of the dataset, the preprocessing procedure and the model architecture are consistent with those in [45]. Therefore, the experimental data labeled as No. 1 are taken directly from that reference. For all other comparative experiments, to ensure fairness in all tests, we used single-channel input data, whereas [45] used randomly generated datasets. Consequently, those results are not adopted from the original paper but are instead based on our reproduced experiments under unified experimental settings.

The results demonstrate that, across the remote sensing datasets used in this study, our model achieves superior performance while using the same or even fewer qubits compared to other quantum models. compared with its classical convolutional counterpart, our proposed model shows a significant improvement in classification accuracy. Furthermore, even compared to the more complex DenseNet model, our model achieves comparable or better classification performance. Hence, relative to the classical baseline, our model exhibits better generalization ability, and when compared with quantum models that employ the same or greater number of qubits, it consistently outperforms them. Against more complex classical models, our method still achieves competitive or superior results.

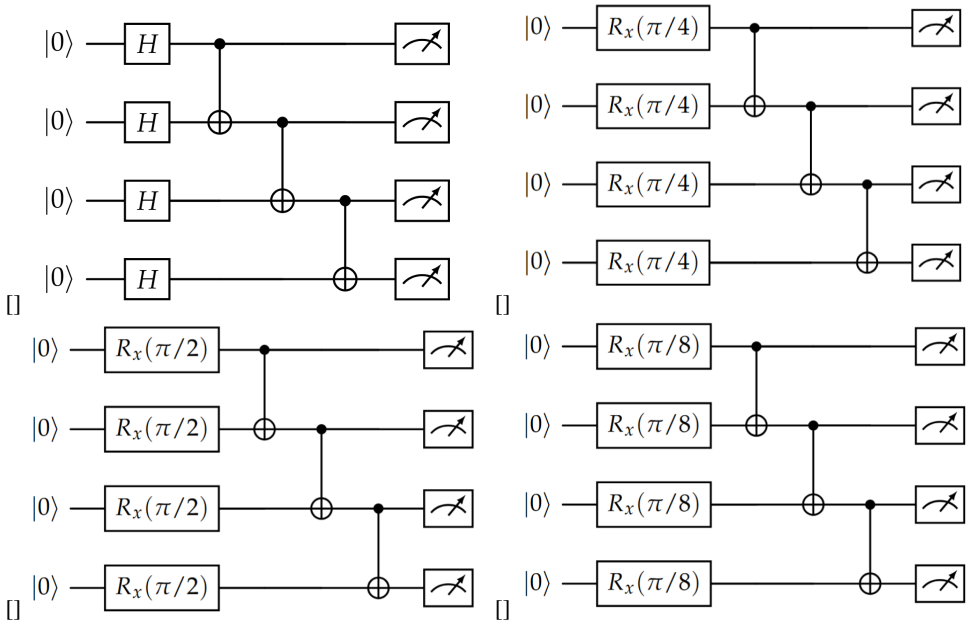

Fig. 6. Four quantum circuits for experimental environment noise evaluation

Table 1. Experimental environment noise assessment

qbit	1		2		3		4	
	Noisy	Ideal	Noisy	Ideal	Noisy	Ideal	Noisy	Ideal
1	0.495 ± 0.0308	0.5	0.1504 ± 0.0181	0.1464	0.5104 ± 0.0268	0.5	0.0547 ± 0.0099	0.38
2	0.4850 ± 0.0343	0.5	0.2630 ± 0.0245	0.25	0.4987 ± 0.0031	0.5	0.0872 ± 0.0124	0.073
3	0.5020 ± 0.0059	0.5	0.3463 ± 0.0490	0.3232	0.5117 ± 0.0326	0.5	0.1237 ± 0.0178	0.106
4	0.5098 ± 0.0174	0.5	0.3893 ± 0.0169	0.375	0.5332 ± 0.0260	0.5	0.1491 ± 0.0250	0.136

Moreover, as shown in Table 2, our model not only attains higher test accuracy but also demonstrates substantially lower standard deviation under quantum noise conditions. This indicates that our model has stronger stability, which is particularly meaningful given that the purity of current quantum systems has not yet reached ideal levels [56].

Coding analysis: Our model is capable of employing multiple types of quantum gates, such as R_X, R_Y, and R_Z, for quantum state encoding. To evaluate the impact of different encoding schemes on classification performance, we conducted a series of experiments in which the R_X, R_Y, and R_Z gates were respectively applied to the quantum encoding circuit. Each experiment was repeated three times, and the mean classification accuracy and standard deviation were computed. The experiments were performed on the OVhead and Pattern datasets described in Section 3.1, using the corresponding dataset configurations, while the experimental setup followed the description in Section 3.3. The results are summarized in Table 3.

As shown in experiments 1–3 and 13–15, the performance of the model when using R_X and R_Y gates for quantum encoding is comparable, indicating that the proposed model does not rely on a specific encoding gate and exhibits robustness with respect to the choice of encoding operation. However, when the R_Z gate is used for encoding, the classification accuracy approaches random guessing, suggesting that the model fails to perform effective learning. Through an analysis of the quantum encoding data, we found that this issue originates from a limitation in the Qiskit framework developed by IBM [51]. Specifically, during the measurement process $qc.measure$, Qiskit cannot directly observe the phase rotation induced by the R_Z operation, resulting in an inability to correctly measure the quantum states that carry convolutional information. Although this limitation falls beyond the primary scope of this study, we nevertheless present the corresponding experimental results to ensure the completeness of our analysis.

The impact of convolution kernel on performance: To evaluate the impact of the number of quantum convolutional kernels on the overall model performance, we conducted experiments using one, two, three, and four quantum convolutional kernels. The experiments were performed on the OVhead and Pattern datasets described in Section 3.1, following the corresponding dataset configurations and the experimental settings outlined in Section 3.3. The results are presented in Table 3, corresponding to experiments 4–7 and 16–19.

When only a single quantum convolutional kernel was employed, the test accuracy on the two datasets decreased by approximately 3% and 2%, respectively, compared with the model using two kernels. In contrast, when three and four convolutional kernels were used, a slight performance degradation of about 1–2% was observed. These results suggest that the performance improvement exhibits diminishing marginal returns with the increasing number of quantum convolutional kernels. Once the model reaches two quantum convolutional kernels, further increasing the kernel count yields negligible or even negative performance gains. Therefore, in the design of quantum convolutional models, blindly increasing the number of convolutional kernels does not necessarily lead to enhanced model performance.

The impact of the number of qubits on classification performance: To investigate the effect of the number of qubits on classification performance, we conducted experiments using 1, 2, 3, and 4 qubits to perform convolution on 9 classical data inputs. When 0 qubits were used, the model degenerated into a classical neural network, specifically a fully connected network. The experiments were performed on the OVhead and Pattern datasets described in Section 3.1, using the corresponding dataset configurations and following the experimental settings in Section 3.3. The results are reported in Table 3, corresponding to experiments 8–12 and 20–24.

Table 2. Model Performance Comparison on Different Datasets.

Dataset	Model	Number	Qubit	Train Acc (%)	Val Acc (%)	Test Acc (%)
Overhead-MNIST [32]	QCNN1 [45]	1	10	69.70±0.40	68.20±0.80	67.20±0.40
	QCNN2 [31]	2	4	82.88±0.67	79.32±0.99	76.56±0.86
	QCNN3 [30]	3	4	68.99±1.88	67.80±1.04	66.35±0.65
	QCNN4 [50]	4	4	95.75±2.16	80.06±0.98	76.19±0.95
	cnn3	5	–	88.90±2.75	77.97±0.72	77.29±1.34
	densnet [48]	6	–	84.42±2.36	83.29±0.20	83.15±0.59
	ours	7	4	96.35±1.81	84.34±0.80	84.46±0.42
Patter-Net [33]	QCNN1 [45]	8	10	91.63±5.02	77.59±1.37	78.15±1.12
	QCNN2 [31]	9	4	86.61±1.50	86.85±1.40	83.98±0.42
	QCNN3 [30]	10	4	68.12±2.24	68.24±4.40	66.57±1.85
	QCNN4 [50]	11	4	97.32±2.49	86.57±1.16	86.20±0.85
	cnn3	12	–	88.23±2.40	83.70±1.53	79.54±1.12
	densnet [48]	13	–	87.50±1.00	87.87±0.58	86.94±0.73
	ours	14	4	93.27±1.40	88.61±0.56	90.56±0.28
RSI-CB256 [34]	QCNN1 [45]	15	10	93.96±2.96	73.06±0.76	73.80±0.47
	QCNN2 [31]	16	4	75.71±1.46	74.06±0.56	71.79±0.93
	QCNN3 [30]	17	4	84.02±3.55	78.70±1.22	79.42±1.62
	QCNN4 [50]	18	4	92.03±1.54	81.64±0.78	79.74±0.68
	cnn3	19	–	89.52±3.61	77.32±1.25	79.98±0.95
	densnet [48]	20	–	89.25±0.48	87.66±0.47	84.59±0.19
	ours	21	4	95.65±0.85	82.27±0.47	84.24±0.33

* Acc stands for accuracy.

It can be observed that as the number of qubits decreases, the information load per qubit increases, leading to a sharp decline in classification performance. Experiments 8 and 20 in Table 3 correspond to the scenario where the proposed quantum model is entirely removed and the preprocessed data is fed directly into the dense layer. In this case, the contribution of our quantum model to classification performance is approximately 5%, demonstrating the effectiveness of the proposed model under current technological conditions.

Table 3. The impact of different modules on model performance

dataset	number	encoding			kernel				qbit					test Acc
		rx	ry	rz	1con	2con	3con	4con	0bit	1bit	2bit	3bit	4bit	
Overhead-MNIST [32]	1	✓				✓							✓	84.4584 ± 0.4153
	2		✓			✓							✓	83.7258 ± 0.7419
	3			✓		✓							✓	17.4254 ± 0.0000
	4	✓			✓								✓	81.2664 ± 0.5943
	5	✓				✓							✓	84.4584 ± 0.4153
	6	✓					✓						✓	83.4642 ± 0.0906
	7	✓						✓					✓	82.5746 ± 1.1320
	8								✓					78.8592 ± 0.3951
	9	✓				✓				✓				42.7525 ± 1.1138
	10	✓				✓					✓			52.7473 ± 2.2146
	11	✓				✓						✓		70.0157 ± 0.8307
	12	✓				✓							✓	84.4584 ± 0.4153
Pattern-Net [33]	13	✓				✓							✓	90.5556 ± 0.2778
	14		✓			✓							✓	90.0000 ± 0.4811
	15			✓		✓							✓	31.6667 ± 0.0000
	16	✓			✓								✓	88.1481 ± 0.4243
	17	✓				✓							✓	90.5556 ± 0.2778
	18	✓					✓						✓	88.9815 ± 0.1604
	19	✓						✓					✓	89.4444 ± 0.4811
	20								✓					83.7037 ± 0.8929
	21	✓				✓				✓				66.4815 ± 1.3981
	22	✓				✓					✓			74.3519 ± 1.1226
	23	✓				✓						✓		82.5000 ± 0.7349
	24	✓				✓							✓	90.5556 ± 0.2778

* Acc stands for accuracy.

4. Discussion

Through comparative experiments in Table 2, we demonstrate that the proposed HAQCCN model exhibits superior classification performance compared with existing quantum and hybrid architectures. Specifically, HAQCCN shows strong adaptability to remote sensing data, effectively capturing spectral–spatial correlations through its hierarchical quantum convolutional kernels. Furthermore, under varying levels of quantum noise, HAQCCN maintains more stable accuracy across different datasets, indicating enhanced robustness of its quantum layers and noise-tolerant encoding strategy.

In contrast, existing hybrid quantum–classical models often suffer from degraded performance when applied to remote sensing data, primarily due to insufficient feature entanglement or limited encoding capacity. They are also more sensitive to hardware-induced quantum noise, leading to fluctuations in measurement outcomes and reduced generalization. These limitations highlight the advantage of our model's design, where the adaptive quantum convolution mechanism and optimized hybrid structure jointly contribute to im-

proved noise resilience and overall classification performance.Moreover, several noteworthy phenomena emerged during the experiments, and these are analyzed in detail below.

As observed in Table 2, experiments 5, 12, and 19 show that the performance of classical convolutional models corresponding to our quantum convolution model is substantially outperformed by our proposed model. However, in experiments 6, 13, and 20, the performance of Densenet is comparable to that of our model. These results indicate that while our model significantly surpasses basic classical schemes, classical deep learning methods remain highly competitive, reflecting decades of development. On the other hand, even at this early stage, deep learning models integrating quantum techniques are already capable of challenging classical approaches. Notably, our model achieves high classification performance using only four qubits. As quantum technology continues to advance rapidly, increasing the number of available qubits will likely enhance the impact of our model across deep learning applications, including remote sensing image classification.

Additionally, we observe that in experiments 11, 17, and 18 of Table 2, our quantum model demonstrates superior performance compared to other quantum models, though its performance is not consistently outstanding across all datasets. Moreover, experiments 1, 8, and 15 show that the Fanfan model exhibits unstable performance, likely because it was originally designed for noiseless environments. The introduction of quantum noise significantly degrades its performance, as noted by the original authors. Another contributing factor may be the low utilization of qubits in its circuit, where quantum gates act on only a subset of qubits while the remaining qubits remain underutilized. Furthermore, after the quantum circuit operates, the system enters a complex entangled state [57], whose potential characteristics are not yet fully understood. Therefore, the observed anomalies in these experiments warrant further investigation, offering insights into the intrinsic properties of quantum circuits and deepening our understanding of quantum computation.

In Table 3, experiments 4–7 and 16–19, we tested the effect of varying the number of quantum convolutional kernels on model performance. When the number of kernels increases, performance does not necessarily improve and may even slightly decline. We attribute this to the increased complexity in feature processing, making it more difficult for the dense layers to capture the relevant information. Similar phenomena have been observed in classical deep learning methods [58–60], but due to quantum entanglement and superposition, the added complexity in quantum convolution can make feature extraction more challenging. Therefore, when using quantum convolutional kernels for feature extraction, excessive quantum operations may obscure features, reducing the effectiveness of downstream layers.

In Table 3, experiments 8–12 and 20–24, we investigated the impact of qubit quantity on classification performance. The results show that decreasing the number of qubits significantly reduces the accuracy of model. However, this reduction does not necessarily imply a deficiency in the feature extraction capability of the quantum circuit; rather, it indicates that a fully connected neural network struggles to utilize these features effectively for classification. These experiments highlight that the number of qubits critically affects quantum convolution-based image classification. Simultaneously, the limited availability of quantum resources restricts the strategy of simply increasing qubit count to improve performance. Accordingly, moving beyond the conventional approach of using a qubit per data element and instead processing more data with fewer qubits becomes a pivotal strat-

egy. Furthermore, this approach is essential for enhancing the computational efficiency of future quantum computers, which represents one of the primary motivations for our proposed model.

5. Conclusions

We present a quantum convolutional architecture capable of encoding a greater volume of classical information while operating with a limited qubit count, resulting in substantially enhanced qubit utilization. In experiments on remote sensing image classification, the approach outperforms existing methodologies. Furthermore, we investigated the effects of quantum encoding techniques, quantum convolutional kernels, and qubit quantity on model performance, providing a more in-depth exploration of the model's internal mechanisms. The proposed model offers a valuable reference for employing quantum computing in remote sensing image recognition and contributes to the advancement of quantum convolutional models.

The results of this research also suggest several avenues for future investigation: (1) developing image encoding and convolution techniques better suited for remote sensing image recognition, (2) exploring strategies to mitigate the problem of qubit information overload under constrained quantum conditions, and (3) designing feature extraction methods specifically tailored for scenarios with qubit information overload.

Acknowledgement. This work is supported by the Scientific Research Fund of National Natural Science Foundation of China (Grant 62372168), the Hunan Provincial Natural Science Foundation of China (Grants 2023JJ30266 and 2025JJ50399), the Research Project on teaching reform in Hunan province (Grant HNJG-2022-0791), the Hunan University of Science and Technology (Grant 2022-448),Key Laboratory of AI and Information Processing, Education Department of Guangxi Zhuang Autonomous Region (Hechi University))(grant 2024GXZDSY010), and the National Social Science Funds of China (Grant 19BZX044).

References

1. Anderson, K., Ryan, B., Sonntag, W., Kavvada, A., Friedl, L.: Earth observation in service of the 2030 agenda for sustainable development. Geo-spatial Information Science 20(2), 77–96 (2017)
2. Ustin, S.L., Middleton, E.M.: Current and near-term advances in earth observation for ecological applications. Ecological Processes 10(1), 1 (2021)
3. Gerasopoulos, E., Bailey, J., Athanasopoulou, E., Speyer, O., Kocman, D., Raudner, A., Tsouni, A., Kontoes, H., Johansson, C., Georgiadis, C., et al.: Earth observation: An integral part of a smart and sustainable city. Environmental Science & Policy 132, 296–307 (2022)
4. McCabe, M.F., Rodell, M., Alsdorf, D.E., Miralles, D.G., Uijlenhoet, R., Wagner, W., Lucieer, A., Houborg, R., Verhoest, N.E., Franz, T.E., et al.: The future of earth observation in hydrology. Hydrology and earth system sciences 21(7), 3879–3914 (2017)
5. Wang, Z., Ma, Y., Zhang, Y., Shang, J.: Review of remote sensing applications in grassland monitoring. Remote Sensing 14(12), 2903 (2022)
6. Chi, M., Plaza, A., Benediktsson, J.A., Sun, Z., Shen, J., Zhu, Y.: Big data for remote sensing: Challenges and opportunities. Proceedings of the IEEE 104(11), 2207–2219 (2016)

7. Zhu, X.X., Tuia, D., Mou, L., Xia, G.S., Zhang, L., Xu, F., Fraundorfer, F.: Deep learning in remote sensing: A comprehensive review and list of resources. IEEE geoscience and remote sensing magazine 5(4), 8–36 (2017)
8. Shi, C., Zhang, X., Sun, J., Wang, L.: Remote sensing scene image classification based on self-compensating convolution neural network. Remote Sensing 14(3), 545 (2022)
9. Xu, X., Li, W., Ran, Q., Du, Q., Gao, L., Zhang, B.: Multisource remote sensing data classification based on convolutional neural network. IEEE Transactions on Geoscience and Remote Sensing 56(2), 937–949 (2017)
10. Zhang, L., Zhang, L.: Artificial intelligence for remote sensing data analysis: A review of challenges and opportunities. IEEE Geoscience and Remote Sensing Magazine 10(2), 270–294 (2022)
11. Zhang, B., Wu, Y., Zhao, B., Chanussot, J., Hong, D., Yao, J., Gao, L.: Progress and challenges in intelligent remote sensing satellite systems. IEEE Journal of Selected Topics in Applied Earth Observations and Remote Sensing 15, 1814–1822 (2022)
12. Cong, I., Choi, S., Lukin, M.D.: Quantum convolutional neural networks. Nature Physics 15(12), 1273–1278 (2019)
13. Ristè, D., Da Silva, M.P., Ryan, C.A., Cross, A.W., Córcoles, A.D., Smolin, J.A., Gambetta, J.M., Chow, J.M., Johnson, B.R.: Demonstration of quantum advantage in machine learning. npj Quantum Information 3(1), 16 (2017)
14. Chen, L., Li, T., Chen, Y., Chen, X., Wozniak, M., Xiong, N., Liang, W.: Design and analysis of quantum machine learning: a survey. Connection Science 36(1), 2312121 (2024)
15. Schumacher, B., Nielsen, M.A.: Quantum data processing and error correction. Physical Review A 54(4), 2629 (1996)
16. Eldar, Y.C., Oppenheim, A.V.: Quantum signal processing. IEEE Signal Processing Magazine 19(6), 12–32 (2002)
17. Senokosov, A., Sedykh, A., Sagingalieva, A., Kyriacou, B., Melnikov, A.: Quantum machine learning for image classification. Machine Learning: Science and Technology 5(1), 015040 (2024)
18. Caraiman, S., Manta, V.I.: Image segmentation on a quantum computer. Quantum Information Processing 14(5), 1693–1715 (2015)
19. Youssry, A., El-Rafei, A., Elramly, S.: A quantum mechanics-based framework for image processing and its application to image segmentation. Quantum Information Processing 14(10), 3613–3638 (2015)
20. Abbas, A., Ambainis, A., Augustino, B., Bärtschi, A., Buhrman, H., Coffrin, C., Cortiana, G., Dunjko, V., Egger, D.J., Elmegreen, B.G., et al.: Challenges and opportunities in quantum optimization. Nature Reviews Physics pp. 1–18 (2024)
21. Liang, W., Liu, Y., Yang, C., Xie, S., Li, K., Susilo, W.: On identity, transaction, and smart contract privacy on permissioned and permissionless blockchain: a comprehensive survey. ACM Computing Surveys 56(12), 1–35 (2024)
22. Hu, N., Zhang, D., Xie, K., Liang, W., Diao, C., Li, K.C.: Multi-range bidirectional mask graph convolution based gru networks for traffic prediction. Journal of Systems Architecture 133, 102775 (2022)
23. Efthymiou, S., Ramos-Calderer, S., Bravo-Prieto, C., Pérez-Salinas, A., García-Martín, D., Garcia-Saez, A., Latorre, J.I., Carrazza, S.: Qibo: a framework for quantum simulation with hardware acceleration. Quantum Science and Technology 7(1), 015018 (2021)
24. Preskill, J.: Quantum computing in the nisq era and beyond. Quantum 2, 79 (2018)
25. Brady, L.T., Baldwin, C.L., Bapat, A., Kharkov, Y., Gorshkov, A.V.: Optimal protocols in quantum annealing and quantum approximate optimization algorithm problems. Physical Review Letters 126(7), 070505 (2021)
26. Herrmann, J., Llima, S.M., Remm, A., Zapletal, P., McMahon, N.A., Scarato, C., Swiadek, F., Andersen, C.K., Hellings, C., Krinner, S., et al.: Realizing quantum convolutional neural

networks on a superconducting quantum processor to recognize quantum phases. Nature communications 13(1), 4144 (2022)
27. Oh, S., Choi, J., Kim, J.: A tutorial on quantum convolutional neural networks (qcnn). In: 2020 International Conference on Information and Communication Technology Convergence (ICTC). pp. 236–239. IEEE (2020)
28. Meng, Y.M., Zhang, J., Zhang, P., Gao, C., Ran, S.J.: Residual matrix product state for machine learning. SciPost Physics 14(6), 142 (2023)
29. Wu, S., Zhang, Y., Li, J.: Quantum data parallelism in quantum neural networks. Physical Review Research 7(1), 013177 (2025)
30. Yang, C.H.H., Qi, J., Chen, S.Y.C., Chen, P.Y., Siniscalchi, S.M., Ma, X., Lee, C.H.: Decentralizing feature extraction with quantum convolutional neural network for automatic speech recognition. In: ICASSP 2021-2021 IEEE International Conference on Acoustics, Speech and Signal Processing (ICASSP). pp. 6523–6527. IEEE (2021)
31. Ovalle-Magallanes, E., Avina-Cervantes, J.G., Cruz-Aceves, I., Ruiz-Pinales, J.: Hybrid classical–quantum convolutional neural network for stenosis detection in x-ray coronary angiography. Expert Systems with Applications 189, 116112 (2022)
32. Noever, D., Noever, S.E.M.: Overhead mnist: A benchmark satellite dataset. arXiv preprint arXiv:2102.04266 (2021)
33. Zhou, W., Newsam, S., Li, C., Shao, Z.: Patternnet: A benchmark dataset for performance evaluation of remote sensing image retrieval. ISPRS journal of photogrammetry and remote sensing 145, 197–209 (2018)
34. Li, H., Dou, X., Tao, C., Wu, Z., Chen, J., Peng, J., Deng, M., Zhao, L.: Rsi-cb: A large-scale remote sensing image classification benchmark using crowdsourced data. Sensors 20(6), 1594 (2020)
35. Xiong, H., Wu, Z., Fan, H., Li, G., Jiang, G.: Quantum rotation gate in quantum-inspired evolutionary algorithm: A review, analysis and comparison study. Swarm and Evolutionary Computation 42, 43–57 (2018)
36. Bataille, M.: Quantum circuits of cnot gates: optimization and entanglement. Quantum Information Processing 21(7), 269 (2022)
37. Liang, W., Li, Y., Xie, K., Zhang, D., Li, K.C., Souri, A., Li, K.: Spatial-temporal aware inductive graph neural network for c-its data recovery. IEEE Transactions on Intelligent Transportation Systems 24(8), 8431–8442 (2022)
38. Liao, J., Guo, L., Jiang, L., Yu, C., Liang, W., Li, K., Pop, F.: A machine learning-based feature extraction method for image classification using resnet architecture. Digital Signal Processing 160, 105036 (2025)
39. Bhat, H.A., Khanday, F.A., Shah, K.A.: Optimal circuit decomposition of reversible quantum gates on ibm quantum computers. In: Handbook of Research on Quantum Computing for Smart Environments, pp. 149–164. IGI Global (2023)
40. Eltschka, C., Huber, M., Morelli, S., Siewert, J.: The shape of higher-dimensional state space: Bloch-ball analog for a qutrit. Quantum 5, 485 (2021)
41. Scholtz, F.G., Geyer, H.B., Hahne, F.: Quasi-hermitian operators in quantum mechanics and the variational principle. Annals of Physics 213(1), 74–101 (1992)
42. Liao, J., Yu, C., Jiang, L., Guo, L., Liang, W., Li, K., Pathan, A.S.K.: A method for composite activation functions in deep learning for object detection. Signal, Image and Video Processing 19(5), 362 (2025)
43. Duchon, C.E.: Lanczos filtering in one and two dimensions. Journal of Applied Meteorology (1962-1982) pp. 1016–1022 (1979)
44. Cerezo, M., Verdon, G., Huang, H.Y., Cincio, L., Coles, P.J.: Challenges and opportunities in quantum machine learning. Nature computational science 2(9), 567–576 (2022)
45. Fan, F., Shi, Y., Guggemos, T., Zhu, X.X.: Hybrid quantum-classical convolutional neural network model for image classification. IEEE transactions on neural networks and learning systems (2023)

46. Fan, F., Shi, Y., Zhu, X.X.: Land cover classification from sentinel-2 images with quantum-classical convolutional neural networks. IEEE Journal of Selected Topics in Applied Earth Observations and Remote Sensing (2024)
47. Sebastianelli, A., Zaidenberg, D.A., Spiller, D., Le Saux, B., Ullo, S.L.: On circuit-based hybrid quantum neural networks for remote sensing imagery classification. IEEE Journal of Selected Topics in Applied Earth Observations and Remote Sensing 15, 565–580 (2021)
48. Huang, G., Liu, Z., Van Der Maaten, L., Weinberger, K.Q.: Densely connected convolutional networks. In: Proceedings of the IEEE conference on computer vision and pattern recognition. pp. 4700–4708 (2017)
49. Hur, T., Kim, L., Park, D.K.: Quantum convolutional neural network for classical data classification. Quantum Machine Intelligence 4(1), 3 (2022)
50. Liu, J., Lim, K.H., Wood, K.L., Huang, W., Guo, C., Huang, H.L.: Hybrid quantum-classical convolutional neural networks. Science China Physics, Mechanics & Astronomy 64(9), 290311 (2021)
51. Javadi-Abhari, A., Treinish, M., Krsulich, K., Wood, C.J., Lishman, J., Gacon, J., Martiel, S., Nation, P.D., Bishop, L.S., Cross, A.W., Johnson, B.R., Gambetta, J.M.: Quantum computing with Qiskit (2024)
52. Ramos Ferreira, F., Fernandes, J.P., Abreu, R.: Quantum software frameworks for deep learning. In: Quantum Software Engineering, pp. 281–302. Springer (2022)
53. Kingma, D.P., Ba, J.: Adam: A method for stochastic optimization. arXiv preprint arXiv:1412.6980 (2014)
54. Jones, M.A., Vallury, H.J., Hill, C.D., Hollenberg, L.C.: Chemistry beyond the hartree–fock energy via quantum computed moments. Scientific Reports 12(1), 8985 (2022)
55. Nation, P.D., Kang, H., Sundaresan, N., Gambetta, J.M.: Scalable mitigation of measurement errors on quantum computers. PRX Quantum 2(4), 040326 (2021)
56. Chen, L., Jia, Z.: On optimum entanglement purification scheduling in quantum networks. IEEE Journal on Selected Areas in Communications 42(7), 1779–1792 (2024)
57. Liu, T.: The applications and challenges of quantum teleportation. In: Journal of Physics: Conference Series. vol. 1634, p. 012089. IOP Publishing (2020)
58. Liu, C.T., Wu, Y.H., Lin, Y.S., Chien, S.Y.: Computation-performance optimization of convolutional neural networks with redundant kernel removal. In: 2018 IEEE international symposium on circuits and systems (ISCAS). pp. 1–5. IEEE (2018)
59. Hu, N., Zhang, D., Xie, K., Liang, W., Li, K., Zomaya, A.: Multi-graph fusion based graph convolutional networks for traffic prediction. Computer Communications 210, 194–204 (2023)
60. Wang, X., Xu, L., Zhou, L., Liu, Y., Xiong, N., Li, K.C.: Large language model-driven probabilistic trajectory prediction in the internet of things using spatio-temporal encoding and normalizing flows. Digital Communications and Networks (2025)

Lianghai Chen is currently pursuing a Master's degree in Software Engineering at Hunan University of Science and Technology. He received his Bachelor's degree in Computer Science and Technology in 2023. His research interests include Quantum Computing and Computer Vision (CV).

Yuzhen Liu is a Lecturer at the School of Computer Science and Engineering, Hunan University of Science and Technology. He received a Ph.D. degree in computational mathematics from Xiangtan University, Xiangtan, Hunan, China, in 2012. He has authored or co-authored about 20 journal/conference papers. His research interests include network security protection and information security.

Yi Lu is currently pursuing a Master's degree in Software Engineering at Hu- nan University of Science and Technology. She received her Bachelor's degree in Com- puter Science and Technology in 2024.Her research interests include Emotional Brain- Computer Interfaces (EBCI)and Computer Vision (CV).

Xiaoliang Wang is a professor of information technology and chair of the Department of Internet of Things Engineering,Hunan University of Science and Technology.He leads a team of researchers and students in Information Security and the Internet of Things,such as VANET security and Anonymous Authentication in Ad Hoc Networks.He received a B.E. in computer engineering from Xiangtan University,China,and a M.S. in computer science from the joint education of Xiangtan University and the Institute of Computing Technology of the Chinese Academy of Sciences,China.He received his Ph.D. from Hunan University. He had worked at Xiangtan University and the Nanjing Government of China and had also worked as a postdoctoral researcher at the University of Alabama.

Huaning Song is an associate professor at Hechi University and the vice dean of the School of Artificial Intelligence and Manufacturing. He is also one of the main members of the Key Laboratory of AI and Information Processing under the Education Department of the Guangxi Zhuang Autonomous Region. He specializes in the application of artificial intelligence models and the development of embedded technologies. He graduated from Guilin University of Electronic Technology with a master's degree in circuits and systems.

Received: October 29, 2025; Accepted: January 13, 2026.